Journal of Magnetic Resonance **157,** 61–68 (2002)
doi:10.1006/jmre.2002.2579

Electron Dipole–Dipole ESEEM in Field-Step ELDOR of Nitroxide Biradicals

L. V. Kulik,* Yu. A. Grishin,* S. A. Dzuba,*,†,[1] I. A. Grigoryev,‡ S. V. Klyatskaya,* S. F. Vasilevsky,* and Yu. D. Tsvetkov*

*Institute of Chemical Kinetics and Combustion, Russian Academy of Sciences, 630090 Novosibirsk, Russia; and †Department of Physics, Novosibirsk State University, 630090 Novosibirsk, Russia; and ‡Novobirsk Institute of Organic Chemistry, 630090 Novosibirsk, Russia

Received December 27, 2001; revised June 3, 2002; published online July 30, 2002

The use of a rapid stepping of the magnetic field for investigation of electron dipole–dipole ESEEM in pulsed X-band ELDOR is described. The magnetic field jump, synchronized with a microwave pumping pulse, is positioned between the second and the third pulses of the stimulated echo pulse sequence. This echo is measured as a function of the delay between the first and the second pulses. The data are analyzed for a Fourier transform resulting in a Pake resonance pattern. To remove the electron-nuclear contributions to ESEEM, time traces with pumping were divided by those without. This resulted in complete elimination of electron-nuclear contributions, which is seen from the absence of peaks at nuclear frequencies and the similarity of results for protonated and deuterated solvents. For increasing the electron–electron modulation depth, a scanning of the magnetic field during the microwave pumping is proposed. The interspin distances and their distribution are determined for two long-chained (ca. 2 nm) nitroxide biradicals in glassy toluene and in frozen nematic liquid crystal 4-cyano-4′-pentyl-biphenyl. For the latter solvent, the alignment of the axis connecting two nitroxides in biradicals is quantitatively analyzed.

Key Words: **ELDOR; biradical; ESEEM; Pake spectrum; dipolar coupling.**

INTRODUCTION

Study of weak magnetic and exchange interactions between unpaired electron spins in solids is now of great interest (*1*). The strength of the magnetic electron dipole–dipole interaction reflects the interspin distance and their mutual orientation in a well-defined way, which allows the study of the radical pair geometry. It becomes especially important with development of biological spin-labeling technology (*2*).

Electron spin echo (ESE) has proved to be a very powerful tool for measuring electron dipole–dipole interaction in long-chained biradicals (distances between two spins larger than 1.5 nm). Several approaches in ESE has been used so far: pulsed electron–electron double resonance (ELDOR) (*3–9*), $2+1$ method (*10–12*), multiple-quantum EPR (*13, 14*), solid-echo and Jeneer–Broekaert sequences (*15*), routine primary ESE envelope modulation (ESEEM), and three-pulse Relaxation-Induced Dipolar Modulation Enhancement (RIDME) experiment (*16*).

The alternative way to perform ELDOR is to switch the magnetic field in the sample volume to a new resonance position (field-step ELDOR). Although this approach was suggested long ago in time-resolved EPR (*17*) and ESE (*18, 19*), it has not been applied so far to study electron–electron interactions. Note that the field-step ELDOR spectrometer is suitable for other types of experiments, e.g., for study of slow molecular motions (*18, 20*).

Field-step ELDOR may be performed with the help of a three-pulse stimulated echo sequence (A. A. Dubinskii, Yu. A. Grishin, and K. Möbius, to be published). The magnetic field jump, along with an additional (fourth) pumping pulse, is positioned between the second and third pulses of the stimulated echo sequence (Fig. 1a). The stimulated echo is measured as a function of the time delay τ between the first and the second pulses. In these experiments the finite magnetic field rise-time does not influence the electron spin coherence.

In this paper we describe our field-step ELDOR setup made on the base of a commercial X-band ESE spectrometer. Applications to study the electron dipole–dipole interactions in nitroxide biradicals are discussed. Pulse sequences for increasing the electron–electron modulation depth and for reducing the dead time are proposed and tested. The way to remove the contribution of electron-nuclear ESEEM is proposed.

THE PULSE SEQUENCES

In the secular approximation for weakly coupled spins, the biradical spin-hamiltonian is

$$H = \omega_A S_{zA} + \omega_B S_{zB} + \omega_{ee} S_{zA} S_{zB}, \qquad [1]$$

where ω_A and ω_B are the Larmor frequencies of the two electron spins in the absence of an interaction between them. In the point-dipole approximation, the electron–electron (ELDOR) frequency is

$$\omega_{ee} = 2/3D(3\cos^2\theta - 1) - 2J, \qquad [2]$$

[1] To whom correspondence should be addressed at Institute of Chemical Kinetics and Combustion, Russian Academy of Sciences, Ul. Institutskaya-3, 630090 Novosibirsk, Russian Federation. E-mail: dzuba@ns.kinetics.nsc.ru.

1090-7807/02 $35.00

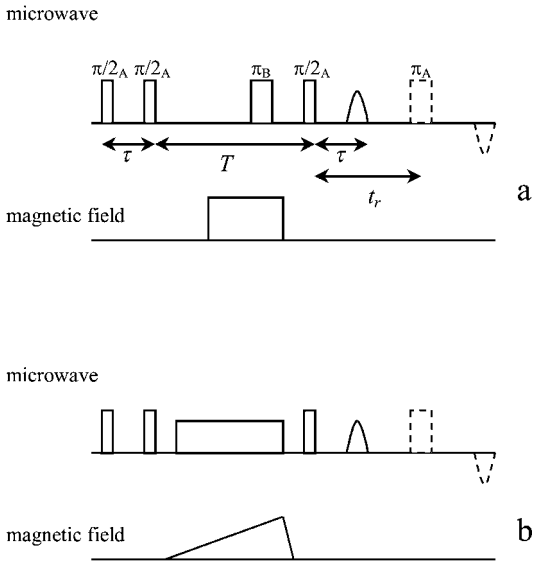

FIG. 1. Pulse sequences for field-step ELDOR. The basic pulse sequence is composed of the three-pulse stimulated echo sequence $\pi/2_A$–τ–$\pi/2_A$–T–$\pi/2_A$–τ–echo and the pumping pulse π_B acting during the field jump. (a) Pumping with fixed magnetic field jump, (b) scanning pumping. To overcome the dead time problem, the echo may be refocused by an additional π_A pulse (dashed line).

where $D = -3/2\gamma^2\hbar/r^3$, γ is the electron gyromagnetic ratio, r is the interspin distance, θ is the angle between the interspin vector and the external magnetic field direction, and J is the exchange interaction. The approximation of weak coupling is valid if $\Delta\omega = |\omega_A - \omega_B| \gg |\omega_{ee}|$ that usually holds for nitroxide biradicals. Anisotropic hyperfine interaction terms are omitted for simplicity.

The simplest four-pulse field-step ELDOR sequence (Fig. 1a) is based on the three-pulse stimulated echo $\pi/2_A$–τ–$\pi/2_A$–T–$\pi/2_A$–τ–echo sequence. As usual, we denote "spin A" as the spins participating in the echo formation and "spin B" as those pumped by an additional pulse. The additional π_B pulse acts during the field jump and thus affects spin B transitions only. The microwave amplitude B_1 is assumed to be large enough to excite both spin A transitions, corresponding to two spin B projections, but small enough not to affect the spin B transitions ($\Delta\omega \gg \gamma B_1 \gg |\omega_{ee}|$).

The first $\pi/2_A$ pulse creates the spin A transverse magnetization which precesses during the first τ-period. The second $\pi/2_A$ pulse converts this transverse magnetization into longitudinal magnetization. The attained phase of precession is conserved during the T-period. The π_B pulse changes the B spin projection and, in consequence, the local dipolar field experienced by spin A alters. Therefore, after the final $\pi/2_A$ pulse the spin A transverse magnetization precesses with a frequency differing by ω_{ee} from its initial value. This results, while τ is varied, in a modulation of the stimulated echo signal:

$$M_y(2\tau + T) \sim \cos(\omega_{ee}\tau). \qquad [3]$$

As the magnetization is stored along the Z-axis during the T-period, the inhomogeneity of the additional magnetic field ΔB does not affect the phase of the observed signal. Another advantage is that the ΔB rise-time that may be as long as $\sim 1\ \mu$s (see below) does not influence the time resolution of the method. Indeed, decay of the stimulated echo for nitroxides at the X-band at 77 K lasts tenths and hundreds of microseconds so one may set the time delay $T > 1\ \mu$s without the loss of the signal.

For a polyoriented sample with the interspin distance fixed, Eq. [3] should be averaged over the angle θ. Its cosine Fourier transform results in a well-known Pake spectrum. From [2] one may obtain two characteristic frequencies, corresponding to $\theta = \pi/2$ and $\theta = 0$:

$$\begin{aligned} f_\perp &= \pm(2/3D + 2J)/2\pi \\ f_\parallel &= \pm(-4/3D + 2J)/2\pi. \end{aligned} \qquad [4]$$

The $f_\perp$ value is determined by the positions of the singularities of the Pake spectrum while the $f_\parallel$ value corresponds to the positions of the outmost edges. So, Eqs. [4] allow the values of D, r, and J to be determined (*21*).

There are, however, some obstacles handicapping the observation of electron–electron ESEEM. First, it is the interference of electron-nuclear ESEEM arising due to anisotropic hyperfine interactions. To overcome this problem, one may assume that electron–electron and electron-nuclear contributions to ESEEM are independent and the latter does not depend on the excitation of B spins. Thus, the pure electron–electron ESEEM may be obtained as a ratio of two experimental traces, with the pumping pulse switched on and off. This procedure removes also the other effects independent of spin B excitation, such as transversal relaxation of spin A.

Another problem is the dipole–dipole ESEEM appearing even in the absence of the pumping, because of the excitation of A spin (*16*). However, this contribution was found to be rather small, even in comparison with electron–proton contribution to ESEEM (*16*). The modulation depth for the latter is known to be much below unity. So, dividing the signal with pumping by that without will result in a correction to Eq. [3] of the second order of smallness. Therefore it may be safely neglected. Note also that in (*16*) the signal was detected at the maximum of an EPR line; any other spectral position will further reduce this spin A contribution to dipole–dipole ESEEM.

Finally, the instrumental dead time, which for an X-band pulse spectrometer is usually about 100 ns, results in a severe distortion of the Pake spectrum. To restore the signal within the dead time, one may apply an additional refocusing π_A pulse (*22*)—see Fig. 1a (dashed line). This pulse is delayed by the time interval t_r after the last $\pi/2_A$ pulse and refocuses the stimulated echo out from the dead time. The ratio of the refocused stimulated echo intensity with the π_B pumping pulse switched on and off should provide the pure electron–electron contribution to ESEEM. Note that for this pulse sequence variation of τ is

restricted, $\tau < t_r$. As the increase of t_r results in signal diminishing, this pulse sequence is suitable to detect only the initial part of the τ-dependence. The dividing two signals, with pumping on and off, scales automatically both types of experiment (4-pulse and 5-pulse) to the same dimensionless amplitude.

The electron–electron modulation depth is proportional to the B spins fraction inverted by the pumping pulse (*7*). For nitroxides at the X-band, with the microwave amplitudes commonly available, this fraction is about 10–20%. This quantity may be substantially increased if the pumping pulse is applied during the ΔB ramp, so that the pumping frequency scans the EPR spectrum (Fig. 1b). To obtain the maximum extent of the spin B inversion, the microwave field amplitude B_1 and the rate of magnetic field variation dB/dt should be matched. The time t_{ex} during which the particular spin B experiences the microwave field, while the external field B is scanned, may be estimated as

$$t_{ex} \approx \frac{B_1}{dB/dt}. \quad [5]$$

For optimal excitation, the turning angle $\gamma t_{ex} B_1 \approx \pi$, so we obtain

$$dB/dt \approx \gamma B_1^2 / \pi. \quad [6]$$

For the usual microwave amplitude, $B_1 = 5$G, that gives $dB/dt \approx 1.3 * 10^8$ G/s (130 G/μs). For complete excitation of the nitroxide X-band EPR line (linewidth ~70 G) the duration of the scanning pumping pulse must be about 0.5 μs.

In addition, the scanning pumping suppresses the ELDOR orientation selectivity (*4*).

EXPERIMENTAL

All experiments were performed with a commercial ESP-380 Bruker pulse EPR spectrometer. A homemade rectangular resonator (mode of oscillations H102) was used.

Conceptually, our equipment for creating the magnetic field jump is similar to that described in (*23*). The field jump was created by the current pulses fed through Helmholtz coils, consisting of two coils of a mean diameter of 24 mm and stuck to resonator side walls. Each coil consists of 3 turns of insulated copper wire. The resonator side walls were made of thin (25 micrometers) foil of nonmagnetic stainless steel, of a specific resistance near 1 Ohm/m/mm^2. The low wall conductivity results in a low Q-value of the resonator, suitable for ESE experiments.

The current pulse circuit is shown in Fig. 2. The module consists of the power supply and the control unit, the high-voltage IC-driver IR 2113, and the transistor half-bridge switch (International Rectifier IRF-NYSE). Components, marked with an asterisk (*), are subject to adjustment; P1, P2, P3 are the reference points for the adjustment of the device; the maximum current is determined by the choice of the resistor R_{LOAD}. The shapes of pulses at the reference points of the device are shown in Fig. 3.

The circuit works as follows. At the initial state the transistors V_1 and V_2 (IRF 730 A), which are controlled by the IC-driver, are closed. The driving rectangular pulse of a duration of $1 \div 3$ μs is produced by a waveform generator triggered by the EPR spectrometer (P1). It opens the transistor V_1 (P1′) and the voltage from the capacitor C_0 is applied to the coils through the ballast resistor R_{LOAD}. The correction chain C_1–R_C–C_2 creates a special shape of the voltage pulse at the output of the switch (P3), to compensate for the distortions of the shape of the current pulse induced by the eddy currents in resonator walls. To reduce the fall time of the coil current, the transistor V_2 is opened for 15 μs (P2) by the end of the input pulse. The resistor R_S is used as a shunt for measuring the parameters of the current pulse in the coil.

The circuit parameters were selected experimentally, to obtain a minimal rise time of the field jump along with its maximal achievable amplitude. The rise and fall times were estimated by measuring the two-pulse echo-detected EPR lineshift (Fig. 3d) and proved to be near 1 μs. In this experiment we used a minimal possible interpulse delay value, $\tau = 80$ ns (so the time resolution of this method was $2\tau = 160$ ns). The current pulse itself has edges about 300 ns (Fig. 3c); the observed elongation

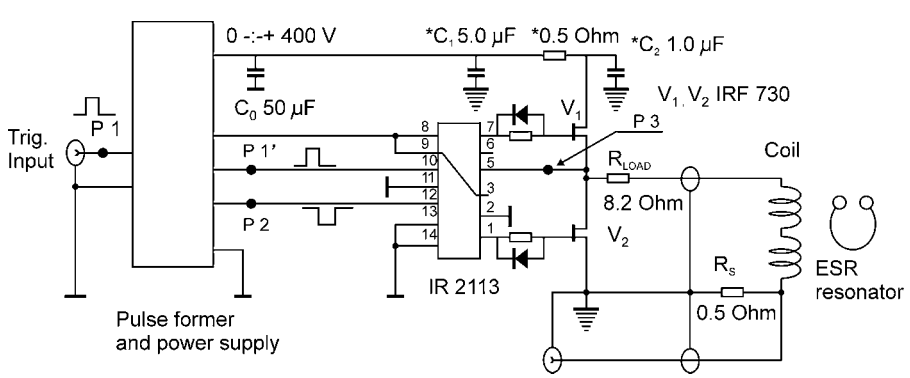

FIG. 2. Schematic diagram of the electronics for generation of magnetic field jumps (see Experimental). P1, P2, P3 are the reference points (see Fig. 3).

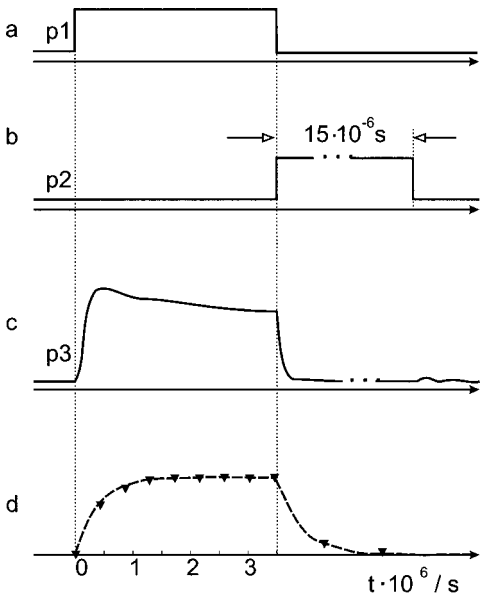

FIG. 3. The time scheme for the voltage and magnetic field pulses. (a) The driving pulse from the waveform generator triggered by the spectrometer (the reference point P1, see Fig. 2); (b) the driving pulse applied to compensate for the distortions induced by the eddy currents in the resonator walls (P2); (c) the output pulse (P3); (d) the echo-detected shift of the EPR resonance.

may be explained by the influence of the eddy currents in the resonator walls. The maximal amplitude of the magnetic field pulse was 70 G, with the load voltage of the capacitor C_0 about 400 volts.

The microwave pulse lengths were 16 and 32 ns for the $\pi/2$ and π pulses, respectively. The echo signal was integrated over a 40-ns time window. Quadrature detection was used, and the modulus signal (square root of the sum of the signals from the both channels squared) was analyzed. This approach is known to reduce the drift of the signal phase due to residual magnetic fields of the eddy currents in the resonator walls (*23*). To remove the nonmodulated contribution to ESEEM, it was fitted by a single exponential function, which was then subtracted.

The spectrometer magnetic field was positioned at the low-field edge of the nitroxide EPR spectrum, while the central maximum of the spectrum was pumped. When the pulse scheme shown in Fig. 1a was employed, the pumping microwave π_B pulse was applied with a delay of 1.3 μs after the magnetic field jump ΔB was switched on. At this moment ΔB almost reaches a plateau (see Fig. 3d); its further variation was less than 0.2 G. In experiments with scanning pumping (Fig. 1b), the maximal ΔB amplitude was about 60 G, and the microwave pumping pulse of 520 ns duration was applied, with a delay of 240 ns after the magnetic field jump was switched on. These values were chosen empirically to obtain a maximum ESEEM depth without affecting the spin A transitions. The delays for the 5-pulse sequence (Fig. 1) were chosen to avoid influence of unwanted echoes.

In our experiments we used biradicals of two types:

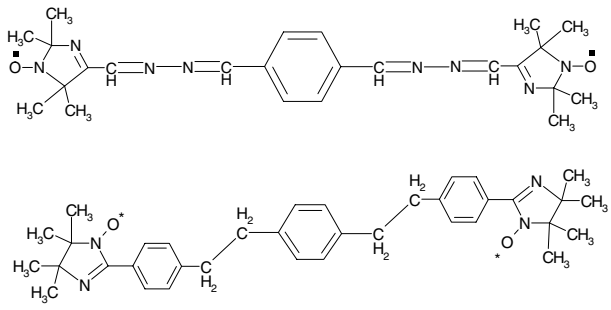

Biradical B1 was synthesized and purified as described in (*24*). The synthesis of biradical B2 will be described in a forthcoming contribution; the procedure closely resembles that given in (*25*).

Biradicals were dissolved in toluene, or in deuterated toluene, or in nematic liquid crystal 5CB (4-cyano-4′-pentyl-biphenyl):

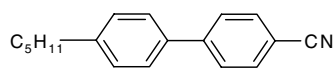

The nitroxide group concentration was 1 mM in all sample preparations.

To obtain a glassy state, the samples of toluene solution were frozen in liquid nitrogen. The samples of liquid crystal solution were slowly cooled in the resonator at the spectrometer field $\mathbf{B_0}$ of 8 kG that resulted in partial orientation of the solvent and biradical molecules along the $\mathbf{B_0}$. Then the samples were frozen in liquid nitrogen. To obtain a desired sample orientation, the sample was turned in the frozen state. All experiments were done at 77 K.

RESULTS AND DISCUSSION

1. Biradical B1: Determination of the Interspin Distance

Figures 4 and 5 show the results of the field-step ELDOR experiment (see Fig. 1, $T = 10$ μs), for B1 in protonated (Fig. 4) and deuterated (Fig. 5) toluene. The solid parts of the curves A and B (curve A, the pumping pulse is on, and curve B, the pumping pulse is off) were obtained in a 4-pulse experiment with scanning pumping (see Fig. 1b). These traces are superimposed by electron-nuclear ESEEM. Curve C presents the ratio of these traces. One can see that curve C looks very similar for both isotope compositions (cf. Figs. 4 and 5). The dashed line on the curves A, B, and C corresponds to the signal obscured within the dead time and obtained using the 5-pulse refocused echo sequence (see Fig. 1b, $t_r = 600$ ns). The joining of data for the 4-pulse and 5-pulse experiments for original traces A and B was done by an appropriate artificial scaling while that for the ratio C occurred automatically after dividing. Note the good agreement for the trace C between two experiments.

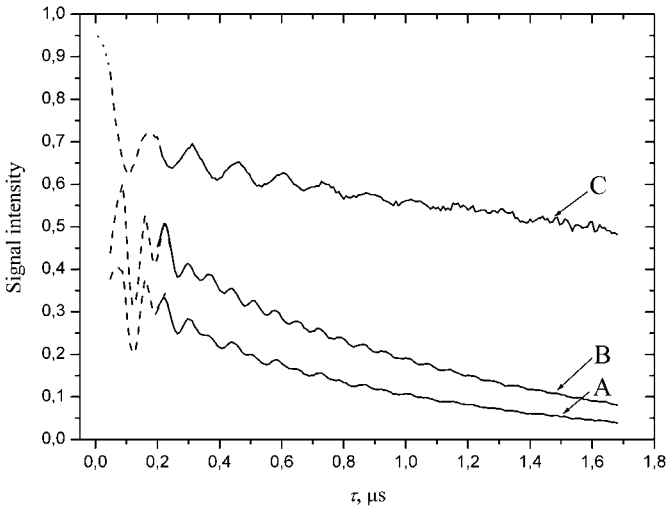

FIG. 4. ESEEM for B1 in toluene (protonated). (A) The four-pulse experiment (solid line) and the five-pulse experiment (dashed line), with the scanning microwave pumping (see Fig. 1b). (B) The same without microwave pumping (pulse π_B is off). (C) The ratio of traces A and B; solid line corresponds to four-pulse experiment; dashed, to the five-pulse experiment. The scale for the solid lines in A and B traces is the same and arbitrary. The scale for the dashed lines in A and B traces is the same; these lines are scaled artificially to match the solid ones. At the vertical axis the dimensionless scale for the C trace is given; the solid and the dashed lines on trace C are scaled to the same values automatically. The dotted line in the trace C is obtained by parabolic extrapolation.

The remaining dead time (~40 ns) is determined by the finite pulse lengths. We reconstructed the signal within that dead time using a simple parabolic interpolation.

The trace D in Fig. 5 was obtained without field scanning (pulse sequence of Fig. 1a). The acquisition parameters for traces C and D were the same. One can see that the modulation depth as well as the signal-to-noise ratio increases when scanning pumping is used.

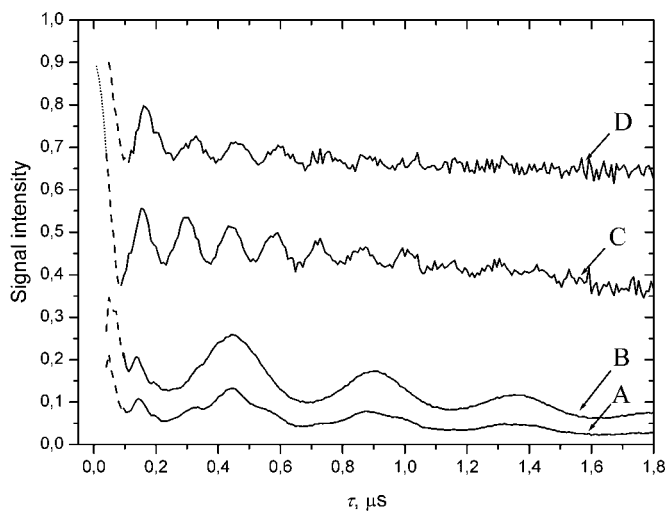

FIG. 5. The same as in Fig. 4, for deuterated toluene (traces A, B, C). The trace D is obtained similarly to the trace C, but with pumping at the fixed field position (see Fig. 1a). The acquisition parameters for traces C and D are the same. One can see that scanning pumping (trace C) increases the modulation depth and signal-to-noise ratio. As compared with Fig. 4, the smaller dead time is because of somewhat higher spin concentration.

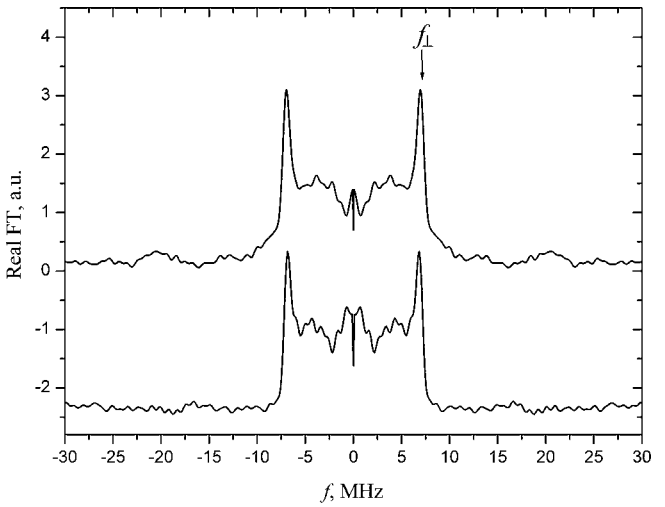

FIG. 6. The Pake spectra obtained by cosine Fourier transform of the traces C on Figs. 5 and 4 (see text for details) for biradical B1 in deuterated (top) and protonated (bottom) toluene. The sharp peaks representing the Pake spectrum singularities are clearly seen. The bottom spectrum is shifted downwards. Note that no spectral features are seen in the frequency region of electron-nuclear ESEEM (for protons near 14.5 MHz) and that both spectra look very similar.

The result of the cosine Fourier transform of the time traces C in Figs. 4 and 5 (with the nonmodulated contribution removed) is shown in Fig. 6. One can see that for both isotope compositions the frequency spectra are almost identical. No peaks are observed corresponding to nuclear transitions. This proves that the suggested approach when two traces, with pumping and without, are divided removes completely the electron-nuclear contribution to ESEEM.

The two symmetric sharp peaks seen in Fig. 6 reflect the singularity of the Pake spectrum at $\theta = \pi/2$. From the position of the peaks the frequency $f_\perp = \pm(7.0 \pm 0.1)$ MHz was determined. Note that $f_\perp$ is shifted slightly from the maximum of singularity; this shift is induced by the line broadening in the frequency domain (*21*). The high-frequency edges ($f_\parallel$) of the Pake spectrum are less pronounced and hardly could be distinguished from noise and artifacts. Their low intensity may be explained by incomplete excitation of the corresponding spin packets because $f_\parallel$, estimated as $2f_\perp$, is close to B_1. In addition, the edges of the Pake spectrum in disordered samples are of rather low intensity.

Intensity of the Pake spectrum edges increases for an oriented sample (*14*). We studied biradical B1 dissolved in 5CB for the sample with the liquid crystal director **d** parallel to $\mathbf{B_0}$. Because of EPR spectrum narrowing, the scanning pumping in these experiments becomes unnecessary. The pumping pulse scheme shown in Fig. 1a was used, with a fixed $\Delta B = 20$ G. Like in the previous case, the traces with the pumping pulse switched on and off were divided and the ratio analyzed. To suppress the

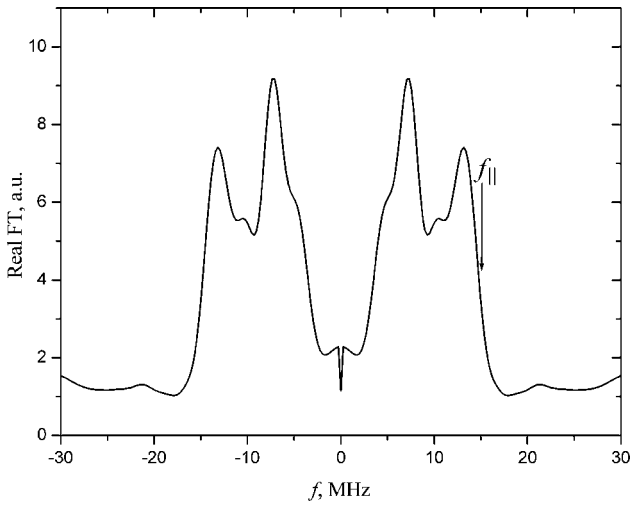

FIG. 7. The Pake spectrum for B1 in 5CB oriented so that $\mathbf{d} \parallel \mathbf{B_0}$, obtained in the same way as that in Fig. 6. Spectral features corresponding to the parallel orientation are increased drastically (cf. Fig. 6).

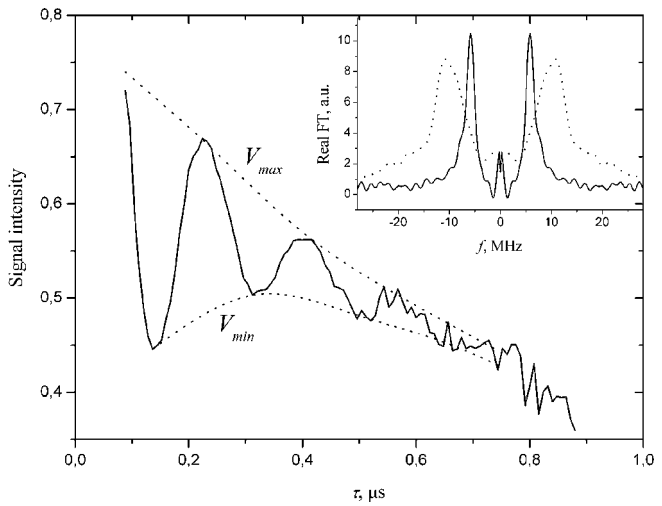

FIG. 8. The time trace obtained in the same way as that for the curve C on Fig. 4, and for B2 in 5CB ($\mathbf{d} \perp \mathbf{B_0}$). The dashed lines represent two envelopes. Inset, the corresponding Pake spectrum (solid line) and that obtained in the same experiment, when $\mathbf{d} \parallel \mathbf{B_0}$ (dashed line).

increasing noise at the tail of the trace, the gaussian apodization function $g(\tau) = \exp(-(2\pi a\tau)^2)$ with the apodization factor $a = 1$ MHz was used (for an expense of some broadening of the resulting Pake spectrum). The Fourier transform is shown in Fig. 7. From the position of the maximum slope at the high frequency edges of the spectrum the value $f_{\parallel} = \pm(14.4 \pm 0.3)$ MHz was determined. With the $f_{\perp}$ determined above (suggesting that it does not depend on the solvent), Eqs. [4] give $D = 10.7 \pm 0.2$ MHz ($r = 1.94 \pm 0.02$ nm), and $|J| < 0.1$ MHz. These results are in excellent agreement with those obtained previously by conventional double-frequency ELDOR: $r = 1.9 \pm 0.16$ nm, $|J| < 2$ MHz (*3*).

2. Biradical B2: Estimation of the Interspin Distance and Its Distribution Width

Electron–electron ESEEM for B2 toluene solution was found to be rather weak, even in the scanning pumping ELDOR experiment. To increase it, we used oriented samples of a liquid crystal solution. The four-pulse scanning pumping pulse scheme (Fig. 1b) was employed. The traces with the pumping pulse on and off, as in the previous case, were divided one by the other. The result is shown in Fig. 8, for $\mathbf{d} \perp \mathbf{B_0}$. The inset in Fig. 8 shows the Fourier transforms obtained for $\mathbf{d} \perp \mathbf{B_0}$ (solid line) and $\mathbf{d} \parallel \mathbf{B_0}$ (dashed line). Ascribing the sharp peaks to the Pake singularities and assuming $J = 0$, the mean interspin distance for B2, $r_m = 2.05$ nm, may be estimated.

One can see that ESEEM oscillations in Fig. 8 are strongly damped, even in this favorite case of oriented sample (cf. Fig. 4). This may be explained as arising from an interspin distance distribution. The B2 chemical structure suggests that a set of conformations may exist.

To estimate the distribution width, we propose the following approach. For τ large enough, ESEEM reflects mainly the Pake spectrum singularity (*7*). Let us introduce the relative modulation amplitude, $A(\tau) = (V_{max}(\tau) - V_{min}(\tau))/V_{max}(\tau)$, where $V_{max}(\tau)$ and $V_{min}(\tau)$ are the two envelopes shown in Fig. 8. The circles in Fig. 9 show $A(\tau)$ for B2 in 5CB; data taken from Fig. 8. For comparison, the triangles show the same dependence for B1 in toluene (data of curve C on Fig. 4). Both dependencies may be approximated by exponential functions, yielding the decay rates $\nu_1 = 1.6 \pm 0.05$ MHz for B1 and $\nu_2 = 4.5 \pm 0.2$ MHz for B2. Suggesting that the interspin distance distribution width, Δr, is small for B1, one may relate the difference $\Delta\nu = \nu_1 - \nu_2$ with the distance distribution for B2. The modulation is determined mainly by the spins in the orientation $\theta \approx \pi/2$, having

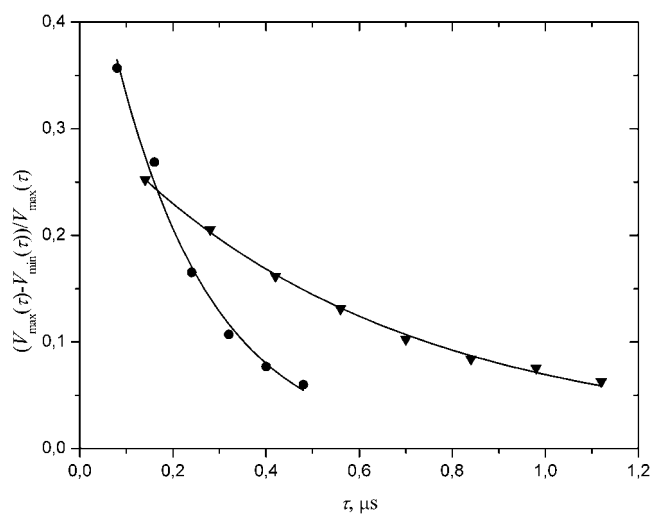

FIG. 9. The relative amplitude of the two envelopes of electron–electron modulation; see Fig. 8 (circles). For comparison, the same data for B1 in toluene (from curve C on Fig. 4) are given by triangles.

the characteristic frequency $f_\perp = 6$ MHz. Because $r \sim f^{-1/3}$, the value $\Delta r \approx r_m^* \Delta\nu/(3f_\perp)$ may be roughly estimated. It gives $\Delta r \approx 0.3$ nm.

3. Alignment of Biradicals in Liquid Crystal

The Pake spectrum for the biradicals B1 and B2 in 5CB allows us to estimate the degree of their orientation with respect to the external magnetic field. One may observe a very pronounced difference, when comparing the Pake spectra for B1 (Fig. 7) and B2 (Fig. 8, dashed line at insert). In both cases, the sample orientation is the same. This difference points out the higher degree of alignment of the biradical molecule for B2.

Note that this type of alignment is perfectly different from that which one might obtain from the EPR spectra alone by analysis of the anisotropic hyperfine coupling. The latter type of alignment deals with orientation of the nitroxide itself while the Pake doublet reflects the alignment of the biradical axis (the axis joining two nitroxides).

To analyze the alignment qualitatively, the order parameter, $S_O = 1/2\langle 3\cos^2\theta - 1\rangle$, may be introduced where the brackets designate the averaging over the ensemble of molecules. It may be estimated from the Pake spectrum in the following way. Let us take into account that the S_O angular dependence is the same as that for the dipolar frequency (in the absence of exchange interaction). Therefore, S_O could be obtained immediately if the lineshape of the single component of the Pake spectrum were known.

Let us designate the component extending from the $f_\perp$ negative to $f_\parallel$ positive as $P_+(f)$, and the symmetric component as $P_-(f)$, $P_-(f) = P_+(-f)$. Then, e.g., employing $P_+(f)$,

$$S_O = \frac{\int f P_+(f)\, df}{4/3|D| \int P_+(f)\, df}. \qquad [7]$$

The actual Pake spectrum is a symmetric combination of the two components $P(f) = P_+(f) + P_-(f)$. One can roughly evaluate the $P_+(f)$ contribution taking into account that $P_+(f) \approx P(f)$, when $f > |f_\perp|$, and $P_+(f) \approx P(f)/2$, in the vicinity of $f \approx 0$. The remaining part of $P_+(f)$ may be obtained by spline interpolation.

Using this reconstruction and Eq. [7], for B1 in toluene solution $S_O = 0.02$ was obtained. That is reasonably close to zero, which one may expect for a polyoriented sample. The values of S_O for B1 and B2 in 5CB ($\mathbf{d} \parallel \mathbf{B_0}$) were found to be 0.38 and 0.67, respectively. Note in this respect that overlapping of the Pake spectrum components is less significant for biradicals in liquid crystal. This means that the distortions imposed by the above procedure here should be smaller.

To explain the higher degree of the B2 alignment, one may take into account that B1 and B2 molecules may interact with the liquid crystal molecules via the π-electrons of the aromatic rings. From this point of view, if two or more aromatic rings are present in the molecular structure, the molecule will be oriented better.

To obtain the precise S_O value by this method, the following precautions should be taken. First, one should avoid in experiment the orientation selectivity. To make results more precise, it is desirable therefore to simulate the Pake spectra taking into account orientation of the nitroxide moieties respectively to the magnetic field (see above), which is beyond the scope of the present paper. Second, the degree of excitation should be equal for all regions of the Pake spectrum ($B_1 > |D|$).

CONCLUSIONS

We examined how an X-band field-step ELDOR may be employed for investigation of the electron dipole–dipole interactions in biradicals. This is an alternative to the conventional double frequency ELDOR that is used in most applications. The advantage is that the scanning pumping increases the ESEEM depth. Also, field-step ELDOR may be easily employed for other types of experiment, such as study of molecular motions (*18, 20*).

To remove the electron-nuclear contributions to ESEEM, time traces with pumping are divided by those without. This results in complete elimination of electron-nuclear contributions, which is seen from the absence of peaks at nuclear frequencies and the similarity of results for protonated and deuterated solvents.

The submicrosecond magnetic field rise time imposed by the technical restrictions is not critical, at least for nitroxides at 77 K. Indeed, this time determines the time interval T between the second and third microwave pulses that may be set as long as T_1. At 77 K, T_1 attains value of several hundreds of microseconds.

In biological applications, singly labeled impurities are often present. As they usually are the same as the monoradical moieties in doubly labeled species, one may expect the same electron-nuclear ESEEM factor in both cases. So, the dividing time traces with pumping and without is applicable here as well. Single nitroxide will produce nonmodulated decay in time domain which is normally removed before Fourier transform.

With this method D and J values were measured for two nitroxide biradicals in isotropic glass and in oriented liquid crystal. The width of the interspin distance distribution for one of them, having more flexible structure, was estimated.

The alignment of biradical molecules in oriented liquid crystal may be studied with this method. We found that interaction of π-electrons between the aromatic rings may be important for this alignment.

ACKNOWLEDGMENTS

The authors are thankful to A. N. Mikhaleva (Novosibirsk Institute of Organic Chemistry) for a kind gift of the liquid crystal 5CB. This work was supported by grants from the Russian Foundation for Basic Research, 00-15-97321 and 00-03-40124, from Ministry of Education of RF, 2000.5.106, and from CRDF (REC-008). L.V.K. acknowledges the INTAS grant for young scientists, YSF 00-99.

REFERENCES

1. "Biological Magnetic Resonance. Vol. 19. Distance Measurements in Biological Systems by EPR" (L. J. Berliner, S. S. Eaton, and G. R. Eaton, Eds.), Kluwer Academic/Plenum, New York (2000).
2. G. L. Millhauser, Selective placement of electron spin resonance spin label: New structural probes for peptides and proteins, *Trends Biochem. Sci*. **17,** 448–468 (1992).
3. A. D. Milov, A. B. Ponomarev, and Yu. D. Tsvetkov, Electron–electron double resonance in electron spin echo: Model biradical systems and sensitized photolysis of decalin, *Chem. Phys. Lett.* **110,** 67–72 (1984).
4. R. J. Larsen and D. J. Singel, Double electron resonance spin echo modulation: Spectroscopic measurement of electron spin pair separations in orientationally disordered solids, *J. Chem. Phys.* **98,** 5134–5146 (1993).
5. H. Hara, A. Kawamori, A.V. Astashkin, and T. Ono, The distances from tyrosine D to redox-active components on the donor side of Photosystem II determined by pulsed electron–electron double resonance, *Biochim. Biophys. Acta* **1276,** 140–146 (1996).
6. V. Pfannebecker, H. Klos, M. Hubrich, T. Volmer, A. Heuer, U. Wiesner, and H. W. Spiess, Determination of end-to-end distances in oligomers by pulsed EPR, *J. Phys. Chem.* **100,** 13428–13432 (1996).
7. A. D. Milov, A. G. Maryasov, and Yu. D. Tsvetkov, Pulsed electron double resonance (PELDOR) and its application in free-radical research, *Appl. Magn. Reson.* **15,** 107–143 (1998).
8. R. E. Martin, M. Pannier, F. Diederich, V. Gramlich, M. Hubrich, and H. W. Spiess, Determination of end-to-end distances in a series of TEMPO diradicals of up to 2.8 nm length with a new four-pulse double electron electron resonance experiment, *Angew. Chem. Int. Ed.* **37,** 2834–2837 (1998).
9. M. Pannier, S. Veit, A. Godt, G. Jeschke, and H. W. Spiess, Dead-time free measurement of dipole–dipole interactions between electron spins, *J. Magn. Reson.* **142,** 331–340 (2000).
10. V. V. Kurshev, A. M. Raitsimring, and Yu. D. Tsvetkov, Selection of dipolar interaction by "2 + 1" pulse train ESE, *J. Magn. Reson.* **81,** 441–451 (1989).
11. A. V. Astashkin, Y. Kodera, and A. Kawamori, Distance between tyrosynes Z^+ and D^+ in plant photosystem-II as determined by pulsed EPR, *Biochim. Biophys. Acta* **1187,** 89–93 (1994).
12. A. V. Astashkin, H. Hara, and A. Kawamori, The pulsed electron–electron double resonance and "2 + 1" study of oriented oxygen-evolving and Mn-depleted preparations of photosystem, II, *J. Chem. Phys*. **108,** 3805–3812 (1998).
13. S. Saxena and J. H. Freed, Double-quantum two-dimensional Fourier transform electron spin resonanse: Distance measurement, *Chem. Phys. Lett.* **251,** 102–110 (1996).
14. P. P. Borbat and J. H. Freed, Multiple quantum ESR and distance measurements, *Chem. Phys. Lett*. **313,** 145–154 (1999).
15. G. Jeschke, M. Pannier, A. Godt, and H. W. Spiess, Dipolar spectroscopy and spin alignment in electron paramagnetic resonance, *Chem. Phys. Lett*. **331,** 243–252 (2000).
16. L. V. Kulik, S. A. Dzuba, I. A. Grigoryev, and Yu. D. Tsvetkov, Electron dipole–dipole interaction in ESEEM of nitroxide biradicals, *Chem. Phys. Lett.* **343,** 315–324 (2001).
17. S. K. Rengen, V. R. Bhagat, and V. S. S. Sastry, Magnetic field-pulsed ELDOR spectroscopy, *J. Magn. Reson.* **33,** 227–240 (1979).
18. S. A. Dzuba and Yu. D. Tsvetkov, Electron spin echo study of slow motions of nitroxide radicals in viscous liquids, *Khim. Fiz.* **1,** 1197–1204 (1982).
19. A. D. Milov, M. D. Zhshirov, and V. E. Khmelinskii, The method of measurement of the electron–electron interaction using magnetic field jump in electron spin echo spectrometer, USSR Certificate of Inventions No. 968719 (1982).
20. S. A. Dzuba, A. G. Maryasov, K. M. Salikhov, and Yu. D. Tsvetkov, Superslow rotations of nitroxide radicals studied by pulse EPR spectroscopy, *J. Magn. Reson*. **58,** 95–117 (1984).
21. S. A. Dzuba, P. Gast, and A. J. Hoff, ESEEM study of spin–spin interactions in spin-polarised $P^+Q_a^-$ pairs in the photosynthetic purple bacterium *Rhodobacter Sphaeroides* R26, *Chem. Phys. Lett.* **236,** 595–602 (1995).
22. C. Schmidt, B. Blümich, and H. W. Spiess, Deuteron two-dimensional exchange NMR in solids, *J. Magn. Reson.* **79,** 269–290 (1988).
23. M. Willer, J. Granwehr, J. Forrer, and A. Schweiger, Two-dimensional nuclear-zeeman-resolved electron spin echo envelope modulation (NZ-ESEEM) spectroscopy, *J. Magn. Reson.* **133,** 46–52 (1998).
24. I. A. Grigoryev, S. A. Dikanov, G. I. Schukin, L. B. Volodarsky, and Yu. D. Tsvetkov, Influence of N-oxyde group in biradicals of imidazoline series on the intramolecular spin exchange via the system of conjugated bonds, *Zh. Struct. Khimii* **23,** No. 6, 59–65 (1982).
25. E. V. Tretyakov, R. I. Samoilova, Yu. I. Ivanov, V. F. Plusnin, S. V. Paschenko, and S. F. Vasilevsky, Stable free imino and nitronil nitroxyl radicals of the acetylene series: Synthesis, electronic absorption spectra and magnetic resonance parameters, *Mendeleev Commun.* **3,** 92–95 (1999).